Published in final edited form as:
Neuron. 2010 March 11; 65(5): 706–717. doi:10.1016/j.neuron.2010.02.021.

Preceding Inhibition Silences Layer 6 Neurons in Auditory Cortex

Yi Zhou[1], **Bao-hua Liu**[1], **Guangying K. Wu**[1], **Young Kim**[1], **Zhongju Xiao**[4], **Huizhong W. Tao**[1,2], and **Li I. Zhang**[1,3]

[1]Zilkha Neurogenetic Institute, University of Southern California, Los Angeles, CA 90089

[2]Department of Cell and Neurobiology, University of Southern California, Los Angeles, CA 90089

[3]Department of Physiology and Biophysics, Keck School of Medicine, University of Southern California, Los Angeles, CA 90089

[4]Department of Physiology, School of Basic Medical Sciences, Southern Medical University, Guangzhou 510515, China

Summary

A canonical feedforward circuit is proposed to underlie sensory cortical responses with balanced excitation and inhibition in layer 4 (L4). However, in another input layer, L6, sensory responses and the underlying synaptic circuits remain largely unclear. Here, cell-attached recordings in rat primary auditory cortex revealed that for the majority of L6 excitatory neurons, tonal stimuli did not drive spike responses, but suppressed spontaneous firings. Whole-cell recordings further revealed that the silencing resulted from tone-evoked strong inhibition arriving earlier than excitation. This pattern of inputs can be attributed to a parallel feedforward circuit with both excitatory and inhibitory inputs disynaptically relayed. In contrast, in the other neurons directly driven by thalamic input, stimuli evoked excitation preceding relatively weak inhibition, resulting in robust spike responses. Thus, the dichotomy of L6 response properties arises from two distinct patterns of excitatory-inhibitory interplay. The parallel circuit module generating preceding inhibition may provide a gating mechanism for conditional corticothalamic feedback.

Introduction

Studies of various adult sensory cortices suggest that neurons receive balanced excitatory and inhibitory inputs activated by sensory stimulation (Moore et al., 1999; Zhang et al., 2003; Wehr and Zador, 2003; Tan et al., 2004; Marino et al., 2005; Okun and Lampl, 2008). In layer 4 (L4) of the auditory cortex, such balance is marked by the similar tuning of excitatory and inhibitory inputs and the relatively constant ratio between their strengths. In addition, stimulation often evokes stereotypic sequence of excitation followed within a few milliseconds by inhibition (Ojima and Murakami, 2002; Zhang et al., 2003; Wehr and Zador, 2003; Tan et al., 2004). Such spectral and temporal relationship between excitation and inhibition can be explained by a canonical feedforward circuit, where the L4 neuron receives direct thalamic excitatory input and disynaptic feedforward inhibitory input from local inhibitory neurons driven by the same set of thalamic inputs (Tan et al., 2004; Gabernet et al., 2005). Under balanced excitation and inhibition, the dynamic range of neuronal representation of sensory stimuli can be broadened (Salinas and Sejnowski, 2000; Turrigiano and Nelson, 2004). The balance has also been proposed to play an important role in shaping receptive field (RF) properties as well as temporal patterns of spike responses. For example, the co-tuned but temporally delayed inhibition will enhance the sharpness of the spike tuning through an iceberg effect (Shamma and Symmes,

Correspondence should be addressed to: L.I.Zhang, liizhang@usc.edu; or Z.Xiao, xiaozj@fimmu.com.

1985; Somers et al., 1995; Anderson et al., 2000; Wang et al., 2002; Zhang et al., 2003; Wehr and Zador, 2003; Tan et al., 2004). In addition, the closely followed inhibition limits the integration window for spike generation, enhancing the precision of spike timing and allowing the neuron to behave as a better coincidence detector for synchronous inputs (Pouille and Scanziani, 2001; Wehr and Zador, 2003; Higley and Contreras, 2006).

However, given the highly diverse response properties of cortical neurons, a simple circuit with balanced excitation and inhibition seems limited for creating the functional diversity (de la Rocha et al., 2008). In the primary auditory cortex (A1), neurons exhibit heterogeneous receptive field properties with respect to frequency and intensity tuning (Schreiner et al., 2000; Sutter and Loftus, 2003), as well as a wide range of temporal response profiles from phasic to sustained responses (Volkov and Galazjuk, 1991; Recanzone, 2000; Wang et al., 2005). Indeed, recent studies have shown that for intensity-tuned neurons, the recruitment of excitation and inhibition as sound intensity increases is unbalanced, and the temporal interval between excitation and inhibition shortens with the increase of intensity (Wu et al., 2006; Tan et al., 2007). In fact, even for non-intensity-tuned neurons, the excitatory-inhibitory balance should be viewed as only approximate, since inhibition exhibits relatively broader frequency tuning than excitation around the best frequency (Wu et al., 2008). Thus, how much the excitatory-inhibitory balance can be generalized to cortical neurons remains to be determined. More importantly, how the precise spectral and temporal interplay between excitatory and inhibitory inputs creates the diverse response properties needs to be further investigated.

Anatomical studies in various species have indicated that thalamocortical axons from the medial geniculate body (MGB) form synapses in both layer 4 and layer 6 of the A1 (Winer et al., 2001; Winer et al., 2005; Llano and Sherman 2008). *In vivo* and *in vitro* recordings also showed that auditory input or thalamic stimulation can elicit responses in layer 6 with the shortest onset latencies (Kaur et al., 2005; Lakatos et al., 2007; Wallace and Palmer 2008), suggesting that layer 6 receives direct thalamic input. Conversely, layer 6 in various primary sensory cortices sends feedback projections predominantly to the first-order thalamic nucleus (i.e. ventral MGB of the auditory thalamus, MGBv) (Ojima 1994; Prieto and Winer, 1999; Winer, 2005; Takayanagi and Ojima, 2006; Rouillller and Welker, 2000; Llano and Sherman 2008), whereas layer 5 neurons projects back to medial and dorsal MGB (MGBd and MGBm) as well as other subcortical nuclei (Games and Winer, 1988; Ojima 1994; Winer, 2005; Takayanagi and Ojima, 2006; Llano and Sherman 2008). It has been proposed that the corticothalamic feedback from layer 6 modulates thalamic responses (Villa et al. 1991; Zhang and Suga 1997; Yan and Ehret 2002), and plays a role in mediating the induction of sound-specific plasticity in the auditory thalamus (Zhang and Suga 2000; Suga and Ma 2003; Zhang and Yan 2008). It is also previously observed that many corticothalamic neurons in layer 6 of cat motor and visual cortices with no clearly responding sensory receptive fileds (Tsumoto and Suda, 1980; Sirota et al., 2005). Compared to layer 4, the synaptic circuitry mechanisms underlying the auditory processing in layer 6 have been poorly understood, partly due to the technical difficulties in recording from neurons in deep layers *in vivo*. In this study, by using cell-attached and whole-cell recordings, we examined the functional properties of L6 neurons and the underlying synaptic mechanisms. We found that tonal stimuli did not drive spike responses in the majority of L6 excitatory neurons, reminiscent of the previous studies (Tsumoto and Suda, 1980; Sirota et al., 2005), but suppressed their spontaneous firings at the expected tonal receptive field. The suppression of evoked spike responses results from a novel synaptic integration pattern with a strong inhibitory input preceding the co-activated excitatory input. Thus, different from layer 4, the layer 6 circuit mainly results in a reversed temporal relationship between excitatory and inhibitory inputs, which can be attributed to a parallel feedforward circuit with both the excitatory and inhibitory inputs disynaptically relayed. Our results suggest that inhibition may play an essential role in creating a wide diversity of response properties, through its specific spectral and temporal patterns inherited from the local cortical

circuitry. Finally, we hypothesize that the specific L6 circuit generating preceding inhibition may provide a gating mechanism for a conditional corticothalamic feedback, which may only be activated under certain circumstances such as conditioning.

Results

Two Types of Spike Responses in Layer 6 Neurons of the Adult A1

We first examined the spike tonal receptive fields (TRFs) of L6 excitatory neurons in the adult rat A1 by loose-patch cell-attached recordings (see Experimental procedures). For each neuron, spike TRF was mapped with 71 × 8 tonal stimuli (see Experimental Procedures) for three to five repetitions. Surprisingly, in a total of 41 randomly recorded regular-spike (RS) neurons (i.e. presumptive excitatory neurons, see Experimental Procedures), tone-driven spike responses were only observed in less than half of them (14 out of 41, named “normal-type”). Twenty-seven neurons could not be driven by tone stimuli (named “silent-type”), although spontaneous firings could be observed. Example neurons are shown in Figure 1A and 1B. The normal-type neuron exhibited a V-shaped spike TRF similar as L4 neurons (Figure 1A), while no spike TRF could be identified for the silent-type neuron (Figure 1B). Instead, in the region of frequency-intensity space where the TRF was expected to appear (as suggested by the recording of local field potentials), the spontaneous firing was clearly suppressed (Figure 1B). We also specifically examined fast-spike (FS) inhibitory neurons by using recording pipettes with a smaller tip (Wu et al., 2008). For FS neurons, the trough-to-peak interval of the spike was 0.34 ± 0.12 ms (mean ± SD, n = 8), whereas it was 0.75 ± 0.18 ms for RS neurons, consistent with previous studies (Mountcastle 1969; Swadlow 1989; Wu et al., 2008; Atencio and Schreiner 2008). All the recorded FS neurons exhibited well-defined spike TRFs, and responded reliably to tone stimuli within their TRF regions (Figure 1C). The L6 normal-type neurons possessed slightly broader spike TRFs than L4 excitatory neurons (Figure 1D, upper panel). The plot of spontaneous versus evoked firing rate revealed that there were two distinct classes of L6 excitatory neurons (Figure 1D, bottom panel). The silent-type neurons although displayed very low levels of evoked responses, exhibited significantly higher spontaneous firing rates than the normal-type neurons ($p < 0.01$, t-test,), indicating that it is unlikely that the absence of tone-evoked responses in these neurons was due to a non-specific reduction of activity level during the experiments. The existence of two classes of L6 neurons was observed under two different anaesthesia conditions and in both sides of the cortex (Figure 1D, bottom panel).

Membrane Potential Responses of Layer 6 Neurons

The existence of two types of L6 responses suggests that the patterns of the underlying synaptic inputs may be distinct. To explore this issue, we carried out current-clamp recordings to examine tone-evoked both supra- and subthreshold membrane potential responses. Figure 2A shows a typical silent-type neuron. It lacked a spike TRF region (Figure 2A, top panel). However, it displayed a clear V-shaped membrane potential response area within which only hyperpolarizing responses were observed (Figure 2A, bottom panel). This explains why the neuron did not exhibit evoked spike responses. In contrast, a normal-type neuron displayed a clear spike TRF, which was narrower than the subthreshold membrane potential response area where depolarizing responses were evoked (Figure 2B). The membrane potential TRF of the normal-type neuron appeared similar to that of L4 neurons (Tan et al., 2004; Wu et al., 2008). The plot of the peak amplitude of the membrane potential response versus the response onset latency for all the recorded neurons again revealed two clusters (Figure 2C). The normal-type neurons exhibited depolarizing responses with shorter onset latencies, while the silent-type neurons displayed hyperpolarizing responses with longer onset latencies ($p < 0.01$, t-test). Thus, the silent-type responses are not due to a lack of synaptic inputs, but to the fact that synaptic inputs result in hyperpolarizing membrane potential responses.

Excitatory and Inhibitory Synaptic inputs to Layer 6 Neurons

What patterns of excitatory and inhibitory synaptic inputs cause hyperpolarizing responses? To address this issue, we applied whole-cell voltage-clamp recordings (see Experimental Procedures). By clamping the cell's membrane potential at -80 mV and 0 mV, levels close to the reversal potentials for $GABA_A$ receptor-mediated Cl^- currents and glutamate receptor-mediated excitatory currents respectively, we obtained TRFs composed of excitatory and inhibitory inputs from the same neuron (see Experimental Procedures). The cell #1 in Figure 3A is shown as an example. It received both excitatory and inhibitory inputs, and the inhibitory TRF roughly matched with the excitatory TRF (Figure 3A), similar to L4 neurons (Zhang et al., 2003; Wehr and Zador, 2003; Tan et al., 2004; Wu et al., 2008). However, its inhibitory input was much weaker than the co-activated excitatory input (Figure 3B). Also similar to L4 responses, the excitatory input preceded the co-activated inhibitory input by a brief interval, and this is the case for almost all the responses evoked by the effective stimuli (Figure 3C). In comparison, in the cell #6, stronger inhibition was elicited than excitation (Figure 3E-F). Interestingly, the temporal relationship between excitation and inhibition was reversed, with the onset latencies of inhibitory responses mostly shorter than the corresponding excitatory responses (Figure 3G). Considering that earlier arriving and strong inhibition may be effective in reducing membrane excitation to levels below the spike threshold, the cell #6 may function like a silent-type neuron as observed in cell-attached recordings.

Since QX314, a blocker of voltage-gated sodium channels, was included in the intracellular solution to improve the quality of voltage-clamp recordings (Nelson et al., 1994; Wu et al., 2006, 2008), we had been unable to experimentally obtain the spike TRFs of the whole-cell recorded neurons. Nonetheless, we derived tone-evoked membrane potential responses by integrating experimentally determined excitatory and inhibitory synaptic conductances in an integrate-and-fire model (see Experimental Procedures). To understand how synaptic inhibition shapes the membrane potential response, we also derived membrane potential responses in the absence of inhibitory input. By setting the spike threshold at 20 mV above the resting membrane potential, we estimated the suprathreshold response region in the frequency-intensity space for the recorded cells. For the cell #1, the membrane potential responses derived from excitatory input alone and from integrating excitatory and inhibitory inputs gave rise to similar spike TRFs (Figure 3D), suggesting that the weak inhibition had minor effects on the size of the spike TRF. In contrast, in the cell #6, while excitatory input alone generated a normally appearing spike TRF, the presence of inhibition had greatly suppressed spike responses, resulting in scattered spikes in the frequency-intensity space and an absence of a clear spike TRF (Figure 3H). Based on these results, it is likely that the cell #1 and cell #6 were functionally a normal-type and silent-type neuron respectively.

Synaptic Mechanisms underlying the Two Types of Layer 6 Responses

We have obtained synaptic responses from a total of 33 presumptive excitatory neurons in layer6 with whole-cell voltage-clamp recordings (see Supplementary Figure 1A-B and Experimental Procedures for discussion). Interestingly, in all of these neurons tone-evoked excitatory responses were observed, indicating that the “silence” of many L6 neurons was not due to an absence of excitatory drive. In 12 of the 33 neurons, we obtained complete excitatory and inhibitory synaptic TRFs. They appeared to separate into two groups, based on the relative strengths of excitatory and inhibitory inputs activated by the same stimulus, as well as the temporal relationship between the two inputs. The first group of neurons (5 out of 12) exhibited similar synaptic input patterns as the cell #1. They received relatively stronger excitation than inhibition, and for most of responses the inhibitory input temporally followed the excitatory input (Figure 4A). On the contrary, the second group (7 out of 12 including the cell #6) received stronger inhibition than excitation, and the inhibitory input mainly preceded the excitatory input (Figure 4B). These synaptic properties suggest that the two groups of neurons are likely

normal-type and silent-type neurons respectively. To summarize the differences between the two groups, 3-4 synaptic responses at and around the best frequency (BF) at 70dB were averaged in order to analyze the response amplitude and onset latency. As shown in Figure 4C, the peak amplitude of inhibition was significantly lower than that of excitation in the normal-type neurons ($p < 0.01$, t-test), but was significantly higher than excitation in the silent-type neurons ($p < 0.01$, t-test). This results in a significant difference in the amplitude ratio of inhibition over excitation (I/E ratio) between the groups (normal-type: 0.5 ± 0.2; silent-type: 3.0 ± 1.5; mean ± S.D.; $p < 0.001$, t-test), while they did not differ significantly in the absolute strength of excitation ($p > 0.2$, t-test). Inhibition displayed a significantly longer onset latency than excitation in the normal-type neurons ($p < 0.01$, paired t-test), but a significantly shorter latency in the silent-type neurons ($p < 0.01$, paired t-test) (Figure 4D). The relative latency of inhibition was -1.62 ± 0.73 ms in the normal-type neurons and 1.58 ± 0.57 ms in the silent-type neurons ($p < 0.001$, t-test). The two groups of neurons were statistically segregated based on the I/E ratio and the relative latency (Figure 4E). We next compared the spike TRFs derived from excitatory input alone and by integrating excitatory and inhibitory inputs for each neuron. In the presence of inhibition, the total frequency responding range of spike responses (at 70dB) was only slightly reduced in the normal-type neurons, but was severely reduced in the silent-type neurons (Figure 4F). These results suggest that the silent-type responses identified in extracellular recordings can be attributed to the stronger inhibition and its earlier onset than excitation, while L4 like synaptic responses with excitation followed by inhibition led to normal spike TRFs in layer 6.

Modelling Outputs from Different Patterns of Synaptic Inputs

To further understand how the amplitude and temporal relationships between excitatory and inhibitory inputs affect the output response, we applied a single-compartment Neuron model to simulate membrane potential responses resulting from different patterns of synaptic inputs, with the temporal profile of modelled synaptic responses derived from our experimental data (see Experimental Procedures). We systematically varied the strength of the inhibitory input, the ratio between the strengths of inhibitory and excitatory inputs (I/E ratio), as well as the interval between the onsets of the two inputs. When the modelled excitatory input (with a 2 nS peak amplitude) precedes a weak inhibitory input (with a 1 nS peak amplitude) by 2 ms, synaptic integration results in a strong membrane depolarization of the cell (Figure 5A, top panel). In comparison, when a strong inhibitory input (6 nS) precedes the excitatory input (2 nS) by 2 ms, synaptic integration results in a hyperpolarization (Figure 5A, bottom panel). With inhibition preceding the excitation by 2ms and the strength of the excitation fixed, increasing the strength of the inhibition monotonically reduces the level of the evoked membrane depolarization, which becomes lower than the spike threshold when the I/E ratio is higher than 0.5 (Figure 5B). Keeping the I/E ratio at 3 but changing the absolute strengths of excitation and inhibition only slightly varies the level of the membrane depolarization (Figure 5C). With the strengths of excitation and inhibition set the same (2 nS and 6 nS), varying the relative latency of inhibition results in a biphasic change in the membrane depolarizing response (Figure 5D). Interestingly, the lowest level of membrane depolarization, or in another word the highest level of suppression, occurs when the inhibitory input precedes the excitatory input by 1.5-2 ms (Figure 5D), which matched the observed temporal delay in the silent-type neurons. Taken together, our modelling results indicate that the level of the membrane depolarizing response is highly sensitive to the ratio between the strengths of excitation and inhibition, as well as their temporal relationship.

Potential Local Circuits in Layer 6

What synaptic circuits can account for the normal and reversed temporal relationships between excitation and inhibition in L6 neurons? To address this issue, we compared the onset latency of spike responses of different types of neurons as well as that of excitatory and inhibitory

synaptic responses in these neurons. Because neurons in the rat A1 mostly exhibit transient/phasic spike responses to tonal stimuli with their onsets precisely time-locked to the onset of stimuli (Wehr and Zador, 2003; Tan et al., 2004), the difference in onset delay may reflect that in the number of relays in the cortical circuit. In L4 excitatory neurons, the onset of inhibitory input is slightly later than that of excitatory input, while it is comparable with the timing of firing of inhibitory neurons in the same layer (Figure 6A, top panel). This is consistent with the canonical feedforward circuit, where L4 inhibitory neurons receive direct thalamic input and provide disynaptic inhibitory input to nearby excitatory neurons (Figure 6D, left). Likely the L4 excitatory neurons need a longer integration time for spike generation, therefore they spike later than nearby inhibitory neurons (Figure 6A, top panel). In L6 normal-type neurons, the onset latencies of excitatory and inhibitory inputs are similar to those in L4 excitatory neurons ($p > 0.5$, t-test), and the onset of excitation is similarly earlier than that of inhibition (Figure 6A, bottom panel). This suggests that a similar feedforward circuit may account for the synaptic inputs to L6 normal-type neurons (Figure 6D, left).

Compared to the normal-type neurons, the onset of excitatory inputs to silent-type neurons is much delayed (Figure 6A, bottom). There are two plausible explanations for this observation: 1) the L6 silent-type neuron does not receive direct thalamic input but receives polysynaptic excitatory input from other cortical neurons; 2) the L6 silent-type neuron receives direct thalamic input, but it is much slower compared to that received by the normal-type neuron due to a slower axonal conduction of impulses and/or slower transmission at thalamocortical synapses. To distinguish these possibilities, we recorded excitatory responses after eliminating intracortical inputs by silencing the cortex with a cocktail of muscimol and SCH90511 (Liu et al., 2007; see Experimental Procedures). Extracellular recordings confirmed that firings of both L4 and L6 neurons were blocked after local cortical injection of the cocktail (see Supplementary Figure 2A-C). Two types of excitatory responses were observed in the silenced cortex. Five out of 14 neurons exhibited fairly normal excitatory TRFs (Figure 6B, top panel), indicating that these neurons received direct thalamic input. Nine neurons did not show evoked excitatory responses at all, although spontaneous synaptic currents were observed (Figure 6B, bottom panel). In the silenced cortex, the remaining excitatory responses displayed short latencies comparable to those of membrane depolarizing and excitatory responses of normal-type neurons in the control cortex (Figure 6C). Excitatory responses with long latencies comparable to those of silent-type neurons were not observed in the silenced cortex (Figure 6C), indicating that the long-latency excitatory responses observed in silent-type neurons can be attributed to intracortical inputs. Based on the above results, we propose a parallel feedforward circuit for L6 silent-type neurons (Figure 6D, right), in which both the excitatory and inhibitory inputs are polysynaptically relayed from the thalamocortical projection. Because the onsets of firings of RS normal-type and FS neurons were similar to those of the excitatory and inhibitory inputs to the silent-type neurons (Figure 6A, bottom panel), it is likely that this circuit module is quadripartite, with the excitation and inhibition disynaptically relayed respectively by RS and FS neurons that are directly driven by thalamic input.

Discussion

Two Distinct Classes of Excitatory Neurons in Layer 6

In this study, *in vivo* cell-attached recordings revealed two functionally distinct classes of excitatory neurons in layer 6. About 60% of recorded excitatory neurons (silent-type) do not exhibit spike TRFs under tonal stimuli, but display reduced spontaneous firing to tones within the expected receptive field region. The other cells (normal-type) exhibit normal spike TRFs similar to L4 neurons. These two classes of neurons can also be identified based on intracellular response properties, such as the level of evoked membrane depolarizations (Figure 2C), the I/E amplitude ratio and the relative synaptic latency (Figure 4E), and likely the onset latency of

the excitatory input *per se* (Supplementary Figure 1C). Previous anatomical studies have shown that L6 neurons in the primary sensory cortices provide feedback projections almost exclusively to the thalamus, and these projections have characteristic small terminals (Ojima 1994; Zhang and Deschênes, 1998; Prieto and Winer, 1999; Rouillller and Welker, 2000; Winer, 2005; Takayanagi and Ojima, 2006; Llano and Sherman 2008). The main target of L6 feedback projections is the first-order thalamic nucleus, which provides ascending input to the primary sensory cortices (Gilbert and Kelly, 1975; Rouillller and Welker, 2000; Llano and Sherman 2008). On the other hand, feedback projections from layer 5 target various subcortical nuclei including higher-order nuclei in the thalamus, and are characterized by giant terminals (Games and Winer, 1988; Ojima 1994; Winer, 2005; Takayanagi and Ojima, 2006; Llano and Sherman 2008). It has been estimated that about 50% of L6 neurons are corticothalamic (CT), about 30-40% are corticocortical (these neurons have axon collaterals restricted to the infragranular laminae), and 10-15% are GABAergic (Gilbert and Kelly, 1975; Zhang and Deschênes, 1997; Zarrinpar and Callaway, 2006; Kumar and Ohana, 2008). To further understand the nature of functionally defined L6 neurons in this study, we reconstructed cell morphologies after the *in vivo* recording. Interestingly, the functionally identified silent-type neurons all exhibited pyramidal cell morphology, with an apical dendrite terminating in layer 4. Their processes have a narrow horizontal span and they extend their processes clearly to the white matter (Supplementary Figure 2D-F). These morphological features are characteristics of the major L6 CT neurons (Zhang and Deschênes, 1997; Zarrinpar and Callaway, 2006; Kumar and Ohana, 2008), suggesting that the silent-type neurons most likely contribute to CT projections. Our finding of silent-type neurons is reminiscent of previous reports in the cat visual and motor cortex that a fraction of L6 CT neurons do not show sensory receptive fields or behaviour-related activity (Tsumoto and Suda, 1980; Sirota et al., 2005).

A Reverse Temporal Sequence: Inhibition Followed by Excitation

Studies from mid-layer excitatory neurons in the A1 suggested that the neurons receive approximately balanced excitatory and inhibitory inputs, as indicated by their similar frequency tunings, similar response amplitudes, a more or less stable amplitude ratio, and a stereotypic temporal relationship with the inhibitory input closely following the coactivated excitatory input (Zhang et al., 2003; Wehr and Zador, 2003; Tan et al., 2004; Wu et al., 2008). This pattern of excitation and inhibition will always result in a transient early depolarization of the membrane potential, but would not lead to a complete suppression of spike responses. For the intensity-tuned neurons located ventral-posterior to the A1, although the recruitment of excitation and inhibition is unbalanced as intensity increases, and the interval between the onsets of excitation and inhibition shortens with the intensity increase, the temporal sequence of excitation and inhibition is kept the same: inhibition follows excitation (Wu et al., 2006). In L6 of the A1, only a minority of neurons exhibit this normal temporal sequence of excitation followed by inhibition. The majority of L6 neurons exhibit a reverse temporal sequence: inhibition precedes excitation. Together with a larger amplitude of inhibition than excitation, tone stimuli can result in a hyperpolarization of the membrane potential, and a complete blockade of spike outputs of these neurons. Our present study has demonstrated a previously unrecognized temporal relationship between sensory-evoked excitation and inhibition. Together with the modelling results, our data suggest that by manipulating the excitatory-inhibitory interplay, diverse functional properties can be created.

Canonical versus Parallel Feedforward Circuit

The canonical microcircuit (Douglas and Martin, 1991) was proposed to account for the response profile of sensory cortical neurons to thalamic stimulation. It was found that thalamic stimulation elicited a transient depolarization followed by a long-lasting hyperpolarization in many neurons cross different layers of the cortex (Douglas and Martin, 1991). The core of the canonical microcircuit is a tripartite feedforward circuit. In layer 4, it involves monosynaptic

thalamic excitatory inputs and disynaptic feedforward inhibitiory inputs from local inhibitory neurons which are driven by the same set of thalamic inputs (Figure 6D, left). Such circuit can largely account for the approximately matched excitatory and inhibitory tunings, as well as the excitation-inhibition sequence and their brief interval. Functionally, the closely following inhibition increases the temporal precision of spike responses and sharpens the frequency selectivity of spike responses (Wehr and Zador, 2003; Tan et al., 2004; Wu et al., 2008). In layer 6, all the neurons exhibit roughly matched excitatory and inhibitory TRFs as L4 neurons, although the best-frequency for inhibition is slightly shifted compared to excitation (Supplementary Figure 1D). However, the canonical feedforward circuit can only apply to a minority of them, which exhibit normal spike TRFs. For the majority of L6 neurons, the reversed temporal relationship between excitation and inhibition fundamentally disagree with the canonical circuit. Since inhibitory inputs derive only from cortical interneurons, the reverse temporal sequence has to be attributed to polysynaptic relays of both excitatory and inhibitory inputs. Functionally, the temporally preceding and strong inhibition primarily silences the neuron's output under normal tonal stimulation.

That the excitatory inputs to silent-type neurons are polysynaptic is supported by the experiments in the silenced cortex. Since L6 neurons in rodent sensory cortices receive intracortical excitatory inputs predominantly from the same layer (Zarrinpar and Callaway 2006; Llano and Sherman 2009), it is likely that the silent-type neurons are driven by the L6 normal-type neurons. It is also possible that they receive excitatory input from L4 neurons, as the reconstructed morphology revealed that their apical dendrites extend to layer 4 (Supplementary Figure 1F), and the spike onset latency of L4 RS neurons is similar to the onset latency of excitatory inputs to silent-type neurons (Figure 6A). Because the onset timing of inhibitory input is similar between silent-type and normal-type neurons (Figure 6A, bottom), it is likely that the silent-type neurons receive inhibition also from L6 FS neurons which are directly driven by thalamic input (Figure 6D, right). Similar as in layer 4 (Wu et al., 2008), the L6 FS neurons spike 1-2 ms earlier than L6 normal-type neurons (Figure 6A, bottom). Thus the inhibitory input arrives 1-2 ms earlier than the excitatory input to silent-type neurons. Such quadripartite parallel feedforward circuit can explain well the largely matched excitatory and inhibitory TRFs with the reversed temporal relationship between excitation and inhibition.

Functional relevance of the proposed layer 6 circuit module

As principal origins of corticothalamic feedback, L6 neurons project back predominantly to the first-order thalamic nucleus (MGBv) and form small “modulator” terminals, whereas L5 neurons project back to higher-order thalamic nuclei (MGBd and MGBm) and form giant “driver” terminals (Ojima 1994; Prieto and Winer, 1999; Winer, 2005; Takayanagi and Ojima, 2006; Rouillller and Welker, 2000; Llano and Sherman 2008). In general, it is thought that L6 CT projections modulate excitatory transmissions of thalamic neurons (Crick, 1984; Sherman and Koch, 1986; Villa et al., 1991; Sillito et al., 1994; Zhang and Suga 1997; Yan and Ehret 2002). However, our recent study showed that sound-evoked spiking activity of thalamic neurons was not significantly affected after silencing of the A1 (Liu et al., 2007), suggesting that the CT feedback may not be directly activated under normal tonal stimulation. The present study further demonstrates that the L6 CT feedback is likely shut off by the strong inhibitory control of L6 silent-type neurons. These studies together address the puzzle that the apparent reciprocal connections made by thalamocortical and corticothalamic projections may lead to a positive feedback loop and result in unstable oscillations (Crick and Koch, 1998; Llano and Sherman 2008).

Under what circumstances can the silent L6 CT projections be activated? One possibility is that these neurons can be activated under specifically structured complex sound that changes the balance between excitation and inhibition. To address this possibility, future studies are

required to examine the dynamic properties of excitatory and inhibitory inputs. Besides that, the CT projections have been proposed to play a role in mediating conditioning-induced sound-specific plasticity in the auditory thalamus (Suga and Ma 2003; Zhang and Yan 2008), which suggests that the CT feedbacks can be activated during pairings of sensory stimulation and attention-related input from the nucleus basalis (NB). Recent studies also suggest that attention (Mitchell et al, 2009) and NB stimulation (Goard and Dan, 2009) can both decorrelate the local intrinsic activity in the cortex, an effect likely mediated by the muscarinic cholinergic system and through inhibitory neurons in the cortex. We thus postulate that only under special circumstances, such as during conditioning, can the strong inhibitory control in layer 6 be relieved and the feedback loop be activated, which then allows the induction of plasticity in the thalamus.

Experimental Procedures

Animal preparation and extracellular recording

All experimental procedures used in this study were approved under the Animal Care and Use Committee at the University of Southern California. Experiments were carried out in a sound-proof booth (Acoustic Systems) as described before (Zhang et al., 2001; Tan et al., 2004; Wu et al., 2006; Wu et al., 2008). Female Sprague-Dawley rats (about 3 months old and weighing 250–300g) were anaesthetized with ketamine and xylazine (ketamine: 45mg/kg; xylazine: 6.4mg/kg; i.p.) or urethane (1.5g/kg). The auditory cortex was exposed and the ear canal on the same side was plugged. Pure tones (0.5–64 kHz at 0.1 octave intervals, 25-ms duration, 3ms ramp) at eight sound intensities (from 0-70 dB SPL, 10 dB interval) were delivered through a calibrated free-field speaker facing the contralateral ear. Multi-unit spikes were recorded with parylene-coated tungsten microelectrodes (2 MΩ, FHC) at 500–600μm below the pia. Electrode signals were amplified (Plexon Inc.) and band-pass filtered between 300 and 6,000 Hz. A custom-made software (LabView, National Instrument) was used to extract the spike times. The number of tone-evoked spikes was counted within a window of 10-30 ms from the onset of tone stimuli. Auditory cortical mapping was carried out by sequentially recording from an array of cortical sites to identify the location and frequency representation of A1. During mapping procedure, the cortical surface was slowly perfused with pre-warmed artificial cerebrospinal fluid (ACSF; in mM: NaCl 124, NaH_2PO4 1.2, KCl 2.5, $NaHCO_3$ 25, Glucose 20, $CaCl_2$ 2, $MgCl_2$ 1) to prevent it from drying.

In vivo whole-cell and cell-attached recordings

After mapping of A1, whole-cell recordings (Moore and Nelson, 1999; Margrie et al., 2002; Zhang et al., 2003; Wehr and Zador, 2003; Tan et al., 2004; Wu et al., 2006, Wu et al., 2008) were obtained from neurons located at 1000–1350μm below the pia, corresponding to layer 6 of the auditory cortex (Winer et al., 2001; Winer et al., 2005; Kaur et al., 2005; Lakatos et al., 2007; Llano and Sherman 2008). This was further confirmed in several experiments with current source density map and nissl staining. We used agar (4%) to minimize cortical pulsation. For voltage-clamp recordings, the pipette (impedance: 4-7 MΩ) solution contained (in mM): 125 Cs-gluconate, 5 TEA-Cl, 4 MgATP, 0.3 GTP, 10 phosphocreatine, 10 HEPES, 1 EGTA, 2 CsCl, 1.5 QX-314, 1% biocytin, pH 7.2. Recordings were made with an Axopatch 200B amplifier (Axon Instruments). The whole-cell and pipette capacitance (30-50 pF) were completely compensated and the initial series resistance (20–50MΩ) was compensated for 50-60% to achieve an effective series resistance of 10-25 MΩ. Signals were filtered at 5 kHz and sampled at 10 kHz. Only neurons with resting membrane potentials lower than -55 mV and with stable series resistance (with < 15% change during the course experiment) were used for further analysis. To obtain tone-evoked synaptic conductances, neurons were clamped at -80mV and then 0mV, which are around the reversal potentials for inhibitory and excitatory currents respectively. For current-clamp recordings, similar recording glass electrodes were

used. The internal solution contained (in mM) 125 K-gluconate, 4 MgATP, 0.3 GTP, 10 phosphocreatine, 10 HEPES, 1 EGTA, pH 7.2, and 1% biocytin. As previously reported and discussed (Moore and Nelson, 1999; Margrie et al., 2002; Wu et al., 2006; Wu et al., 2008), the whole-cell recordings under our recording conditions (with large tip size) target exclusively pyramidal neurons. The quality of voltage-clamp in our recordings was reasonably good, as shown by the linear I-V relationship for the recorded synaptic currents, as well as the match to the expected reversal potential of excitatory currents when the recorded synaptic currents were measured within a 1 ms window right after the onset of synaptic responses under hyperpolarized potentials (see Supplementray Figure 1A).

Cell-attached recording was used to characterize the spike responses from individual neurons. Pipettes with smaller tip openings (impedance:~10 MΩ; Wu et al., 2008). The same intra-pipette solution as that in current-clamp recordings was used. Cell-attached recordings were performed in a similar way as whole-cell recordings, except that a loose seal (0.1–0.5 giga Ohm) was made from neurons, allowing spikes only from the patched cell to be recorded. Recording was under voltage-clamp mode and holding voltage was adjusted to obtain a zero baseline current. Signals were filtered at 10 kHz to record both local field potentials and spike responses. Spike shapes were determined by custom-developed LabView software to identify the FS and RS cell types. In a few experiments, after identifying the functional class of the recorded cells, the cell-attached recording was followed by breaking in the cell membrane to load the cell with biocytin (Supplementary Figure 2F). Normal histological procedures were then followed to reconstruct the morphology of the recorded cell.

Cortical silencing

The cortex was pharmacologically silenced following the method established in our previous study (Liu, et al., 2007). A cocktail of SCH50911(6 mM; a specific antagonist of $GABA_B$ receptors) and muscimol (4mM; an agonist of $GABA_A$ receptor) was used to effectively silence a relatively large cortical region. The cocktail (dissolved in ACSF containing Fast Green) were injected through a glass micropipette with a tip opening of 2–3 μm in diameter. The pipette was inserted to a depth of 800 mm beneath the cortical surface. Solutions were injected under a pressure of 3–4 psi for 5 min. The injected volume was estimated to be around 50-100 nl, as measured with mineral oil. The staining by Fast Green was monitored under the surgical microscope, which covered a cortical area with a radius of ~1 mm by the end of the injection.

Data analysis

Synaptic conductances

Excitatory and inhibitory synaptic conductances were derived according to (Borg-Graham et al., 1998; Anderson et al., 2000; Zhang et al., 2003; Wehr and Zador, 2003; Wu et al., 2006):

$$I(t)=Gr(V_m(t)-Er)+Ge(t)(V_m(t)-Ee)+Gi(t)(V_m(t)-Ei).$$

I is the amplitude of synaptic current at any time point. G_r and E_r are the resting conductance and resting membrane potential which were derived from the baseline current of each recording. G_e and G_i are the excitatory and inhibitory synaptic conductance respectively. V is the holding voltage, and E_e (0 mV) and E_i (-80 mV) are the reversal potentials. In this study, a corrected clamping voltage was used, instead of the holding voltage applied (V_h). $V(t)$ is corrected by $V(t) = V_h - Rs*I(t)$, where Rs was the effective series resistance. A 10 mV junction potential was corrected. By holding the recorded cell at two different voltages, G_e and G_i were calculated from the equation. G_e and G_i reflect the strength of pure excitatory and inhibitory synaptic inputs, respectively. Under holding potentials of –80 mV, activation of NMDA

receptors could be ignored (Jahr and Stevens, 1990a; Jahr and Stevens, 1990b; Pinault, 1996). Thus the recorded tone-evoked synaptic currents were primarily mediated by AMPA and $GABA_A$ receptors.

Tone-evoked responses

A) Spike responses. With cell-attached recording, spikes can be detected without ambiguity because their amplitudes are normally higher than 100 pA, while the baseline fluctuation is less than 5 pA. Tone-driven spikes were identified within a 10-30 ms time window after the onset of the tone stimuli. The spike response latency was defined as the lag between the stimulus onset and the negative peak for the first evoked spike. The onset latency of spike responses for a cell was then chosen as the value at 5% position of the cumulative histogram of all the response latencies. B) Synaptic responses. These responses were identified according to their onset latencies and peak amplitudes. All the response traces evoked by the same test stimulus were averaged, and the onset latency of this average trace was identified at the time point in the rising phase of the response wave form, where the amplitude was larger than 3 folds of standard deviation of the baseline. Only responses with onset latencies within 7-30 ms from the onset of tone stimulus were considered in this study.

Deriving membrane potential responses

Membrane potential and spike responses were derived from the recorded excitatory and inhibitory responses based on an integrate-and-fire model (Wehr et al., 2003; Liu et al., 2007; Somers et al. 1995):

$$V_m(t+dt) = -\frac{dt}{C}[G_e(t) * (V_m(t) - E_e) + G_i(t) * (V_m(t) - E_i) + G_r(V_m(t) - E_r)] + V_m(t)$$

where $V_m(t)$ is the membrane potential at time t, C the whole-cell capacitance, G_r the resting leaky conductance, E_r the resting membrane potential (-65 to -60mV). To simulate spike responses, 20mV above the resting membrane potential was set as the spike threshold and a 10ms refractory period was used. Based on the synaptic inputs, a tone stimulus only generated one spike response. C was measured during experiments and G_r was calculated based on the equation $G_r = C*G_m/C_m$, where G_m, the specific membrane conductance is $2e^{-5}$ S/cm^2, and C_m, the specific membrane capacitance is $1e^{-6}$ F/cm^2 (Hines, 1993).

Modelling

The synaptic inputs to a pyramidal neuron in layer 6 were simulated by the following equation (Zhang et al., 2003):

$$I(t) = a \cdot H(t - t_0) \cdot \left(1 - e^{-(t-t_0)/\tau_{rise}}\right) \cdot e^{-(t-t_0)/\tau_{decay}}$$

$I(t)$ is the modelled synaptic current; a is the amplitude factor; $H(t)$ is the Heaviside step function; t_0 is the onset delay of excitatory or inhibitory input. τ_{rise} and τ_{decay} define the shape of the rising phase and decay of the synaptic current. The τ_{rise} and τ_{decay} were chosen by fitting the average shape of recorded synaptic responses with the above function. The t_0 and a are chosen based on our experimental data.

Supplementary Material

Refer to Web version on PubMed Central for supplementary material.

Acknowledgments

This work was supported by grants to L.I.Z. from the US National Institutes of Health/National Institute on Deafness and Other Communication Disorders (R01DC008983, R21DC008588), the Searle Scholar Program, the Klingenstein Foundation, and the David and Lucile Packard Foundation (Packard Fellowships for Science and Engineering). Z.Xiao is supported by National Natural Science Foundation of China (Grant Nos. 30730039, 30970982, and 30670665).

References

Anderson JS, Carandini M, Ferster D. Orientation tuning of input conductance, excitation, and inhibition in cat primary visual cortex. J Neurophysiol 2000;84:909–926. [PubMed: 10938316]

Atencio CA, Schreiner CE. Spectrotemporal processing differences between auditory cortical fast-spiking and regular-spiking neurons. J Neurosci 2008;28:3897–3910. [PubMed: 18400888]

Borg-Graham LJ, Monier C, Frégnac Y. Visual input evokes transient and strong shunting inhibition in visual cortical neurons. Nature 1998;393:369–373. [PubMed: 9620800]

Crick F. Function of the thalamic reticular complex: the search-light hypothesis. Proc Natl Acad Sci USA 1984;81:4586–4590. [PubMed: 6589612]

Crick F, Koch C. Constraints on cortical and thalamic projections: the no-strong-loops hypothesis. Nature 1998;391:245–250. [PubMed: 9440687]

de la Rocha J, Marchetti C, Schiff M, Reyes AD. Linking the response properties of cells in auditory cortex with network architecture: cotuning versus lateral inhibition. J Neurosci 2008;28:9151–63. [PubMed: 18784296]

Douglas RJ, Martin KA. A functional microcircuit for cat visual cortex. J Physiol 1991;440:735–769. [PubMed: 1666655]

Gabernet L, Jadhav SP, Feldman DE, Carandini M, Scanziani M. Somatosensory integration controlled by dynamic thalamocortical feed-forward inhibition. Neuron 2005;48:315–27. [PubMed: 16242411]

Games KD, Winer JA. Layer V in rat auditory cortex: projections to the inferior colliculus and contralateral cortex. Hear Res 1988;34:1–25. [PubMed: 3403382]

Gilbert CD, Kelly JP. The projections of cells in different layers of the cat's visual cortex. J Comp Neurol 1975;163:81–105. [PubMed: 1159112]

Goard M, Dan Y. Basal forebrain activation enhances cortical coding of natural scenes. Nat Neurosci 2009;12:1444–9. [PubMed: 19801988]

Higley MJ, Contreras D. Balanced excitation and inhibition determine spike timing during frequency adaptation. J Neurosci 2006;26:448–57. [PubMed: 16407542]

Hines, M. NEURON–a program for simulation of nerve equations Neural Systems: Analysis and Modeling. Eeckman, FH., editor. MA: Kluwer press; 1993. p. 127-136.

Jahr CE, Stevens CF. A quantitative description of NMDA receptor-channel kinetic behavior. J Neurosci 1990;10:1830–1837. [PubMed: 1693952]

Jahr CE, Stevens CF. Voltage dependence of NMDA-activated macroscopic conductances predicted by single-channel kinetics. J Neurosci 1990;10:3178–3182. [PubMed: 1697902]

Kaur S, Rose HJ, Lazar R, Liang K, Metherate R. Spectral integration in primary auditory cortex: laminar processing of afferent input, in vivo and in vitro. Neuroscience 2005;134:1033–1045. [PubMed: 15979241]

Kumar P, Ohana O. Inter- and intralaminar subcircuits of excitatory and inhibitory neurons in layer 6a of the rat barrel cortex. J Neurophysiol 2008;100:1909–22. [PubMed: 18650305]

Lakatos P, Chen CM, O'Connell MN, Mills A, Schroeder CE. Neuronal oscillations and multisensory interaction in primary auditory cortex. Neuron 2007;53:279–292. [PubMed: 17224408]

Liu BH, Wu GK, Arbuckle R, Tao HW, Zhang LI. Defining cortical frequency tuning with recurrent excitatory circuitry. Nat Neurosci 2007;10:1594–1600. [PubMed: 17994013]

Llano DA, Sherman SM. Evidence for nonreciprocal organization of the mouse auditory thalamocortical-corticothalamic projection systems. J Comp Neurol 2008;10:1209–1227. [PubMed: 18181153]

Llano DA, Sherman SM. Differences in intrinsic properties and local network connectivity of identified layer 5 and layer 6 adult mouse auditory corticothalamic neurons support a dual corticothalamic projection hypothesis. Cereb Cortex. 2009 April 7, 2009.

Margrie TW, Brecht M, Sakmann B. In vivo, low-resistance, whole-cell recordings from neurons in the anaesthetized and awake mammalian brain. Pflugers Arch 2002;444:491–498. [PubMed: 12136268]

Marino J, Schummers J, Lyon DC, Schwabe L, Beck O, Wiesing P, Obermaver K, Sur M. Invariant computations in local cortical networks with balanced excitation and inhibition. Nat Neurosci 2005;8:194–201. [PubMed: 15665876]

Mitchell JF, Sundberg KA, Reynolds JH. Spatial attention decorrelates intrinsic activity fluctuations in macaque area V4. Neuron 2009;63:879–88. [PubMed: 19778515]

Moore CI, Nelson SB, Sur M. Dynamics of neuronal processing in rat somatosensory cortex. Trends Neurosci 1999;22:513–520. [PubMed: 10529819]

Mountcastle VB, Talbot WH, Sakata H, Hyvarinen J. Cortical neuronal mechanisms in flutter-vibration studied in unanesthetized monkeys. Neuronal periodicity and frequency discrimination. J Neurophysiol 1969;32:452–484. [PubMed: 4977839]

Nelson S, Toth L, Sheth B, Sur M. Orientation selectivity of cortical neurons during intracellular blockade of inhibition. Science 1994;265:774–777. [PubMed: 8047882]

Ojima H. Terminal morphology and distribution of corticothalamic fibers originating from layers 5 and 6 of cat primary auditory cortex. Cereb Cortex 1994;4:646–63. [PubMed: 7703690]

Ojima H, Murakami K. Intracellular characterization of suppressive responses in supragranular pyramidal neurons of cat primary auditory cortex in vivo. Cereb Cortex 2002;12:1079–1091. [PubMed: 12217972]

Okun M, Lampl I. Instantaneous correlation of excitation and inhibition during ongoing and sensory-evoked activities. Nat Neurosci 2008;11:535–7. [PubMed: 18376400]

Pinault D. A novel single-cell staining procedure performed in vivo under electrophysiological control: morpho-functional features of juxtacellularly labeled thalamic cells and other central neurons with biocytin or Neurobiotin. J Neurosci Methods 1996;65:113–136. [PubMed: 8740589]

Pouille F, Scanziani M. Enforcement of temporal fidelity in pyramidal cells by somatic feed-forward inhibition. Science 2001;293:1159–1163. [PubMed: 11498596]

Prieto JJ, Winer JA. Layer VI in cat primary auditory cortex: Golgi study and sublaminar origins of projection neurons. J Comp Neurol 1999;404:332–58. [PubMed: 9952352]

Recanzone GH. Response profiles of auditory cortical neurons to tones and noise in behaving macaque monkeys. Hear Res 2000;150:104–118. [PubMed: 11077196]

Rouiller EM, Welker E. A comparative analysis of the morphology of corticothalamic projections in mammals. Brain Res Bull 2000;53:727–41. [PubMed: 11179837]

Salinas E, Sejnowski TJ. Impact of correlated synaptic input on output firing rate and variability in simple neuronal models. J Neurosci 2000;20:6193–6209. [PubMed: 10934269]

Sherman SM, Koch C. The control of retinogeniculate transmission in the mammalian lateral geniculate nucleus. Exp Brain Res 1986;63:1–20. [PubMed: 3015651]

Schreiner CE, Read HL, Sutter ML. Modular organization of frequency integration in primary auditory cortex. Annu Rev Neurosci 2000;23:501–529. [PubMed: 10845073]

Shadlen MN, Newsome WT. Noise, neural codes and cortical organization. Curr Opin Neurobiol 1994;4:569–579. [PubMed: 7812147]

Shamma SA, Symmes D. Patterns of inhibition in auditory cortical cells in awake squirrel monkeys. Hear Res 1985;19:1–13. [PubMed: 4066511]

Shu Y, Hasenstaub A, McCormick DA. Turning on and off recurrent balanced cortical activity. Nature 2003;423:288–293. [PubMed: 12748642]

Sillito AM, Jones HE, Gerstein GL, West DC. Feature-linked synchronization of thalamic relay cell firing induced by feedback from the visual cortex. Nature 1994;369:479–82. [PubMed: 8202137]

Sirota MG, Swadlow HA, Beloozerova IN. Three channels of corticothalamic communication during locomotion. J Neurosci 2005;25:5915–25. [PubMed: 15976080]

Somers DC, Nelson SB, Sur M. An emergent model of orientation selectivity in cat visual cortical simple cells. J Neurosci 1995;15:5448–5465. [PubMed: 7643194]

Suga N, Ma X. Multiparametric corticofugal modulation and plasticity in the auditory system. Nat Rev Neurosci 2003;4:783–794. [PubMed: 14523378]

Sutter ML, Loftus WC. Excitatory and inhibitory intensity tuning in auditory cortex: evidence for multiple inhibitory mechanisms. J Neurophysiol 2003;90:2629–2647. [PubMed: 12801894]

Swadlow HA. Efferent neurons and suspected interneurons in S-1vibrissa cortex of the awake rabbit: receptive fields and axonal properties. J Neurophysiol 1989;62:288–308. [PubMed: 2754479]

Takayanagi M, Ojima H. Microtopography of the dual corticothalamic projections originating from domains along the frequency axis of the cat primary auditory cortex. Neuroscience 2006;142:769–780. [PubMed: 16890371]

Tan AY, Zhang LI, Merzenich MM, Schreiner CE. Tone-evoked excitatory and inhibitory synaptic conductances of primary auditory cortex neurons. J Neurophysiol 2004;92:630–643. [PubMed: 14999047]

Tsumoto T, Suda K. Three groups of cortico-geniculate neurons and their distribution in binocular and monocular segments of cat striate cortex. J Comp Neurol 1980;193:223–36. [PubMed: 7430428]

Turrigiano GG, Nelson SB. Homeostatic plasticity in the developing nervous system. Nat Rev Neurosci 2004;5:97–107. [PubMed: 14735113]

Villa AE, Rouiller EM, Simm GM, Zurita P, de Ribaupierre Y, de Ribaupierre F. Corticofugal modulation of the information processing in the auditory thalamus of the cat. Exp Brain Res 1991;86:506–517. [PubMed: 1761088]

Volkov IO, Galazjuk AV. Formation of spike response to sound tones in cat auditory cortex neurons: interaction of excitatory and inhibitory effects. Neuroscience 1991;43:307–321. [PubMed: 1922775]

Wallace MN, Palmer AR. Laminar differences in the response properties of cells in the primary auditory cortex. Exp Brain Res 2008;184:179–191. [PubMed: 17828392]

Wang J, McFadden SL, Caspary D, Salvi R. Gamma-aminobutyric acid circuits shape response properties of auditory cortex neurons. Brain Res 2002;944:219–231. [PubMed: 12106684]

Wang X, Lu T, Snider RK, Liang L. Sustained firing in auditory cortex evoked by preferred stimuli. Nature 2005;435:341–346. [PubMed: 15902257]

Wehr M, Zador AM. Balanced inhibition underlies tuning and sharpens spike timing in auditory cortex. Nature 2003;426:442–446. [PubMed: 14647382]

Winer JA, Diehl JJ, Larue DT. Projections of auditory cortex to the medial geniculate body of the cat. J Comp Neurol 2001;430:27–55. [PubMed: 11135244]

Winer JA, Miller LM, Lee CC, Schreiner CE. Auditory thalamocortical transformation: structure and function. Trends Neurosci 2005;28:255–263. [PubMed: 15866200]

Winer JA. Decoding the auditory corticofugal systems. Hear Res 2005;207:1–9. [PubMed: 16091301]

Wu GK, Li P, Tao HW, Zhang LI. Nonmonotonic synaptic excitation and imbalanced inhibition underlying cortical intensity tuning. Neuron 2006;52:705–715. [PubMed: 17114053]

Wu GK, Arbuckle R, Liu BH, Tao HW, Zhang LI. Lateral sharpening of cortical frequency tuning by approximately balanced inhibition. Neuron 2008;58:132–143. [PubMed: 18400169]

Yan J, Ehret G. Corticofugal modulation of midbrain sound processing in the house mouse. Eur J Neurosci 2002;16:119–128. [PubMed: 12153536]

Zarrinpar A, Callaway EM. Local connections to specific types of layer 6 neurons in the rat visual cortex. J Neurophysiol 2006;95:1751–1761. [PubMed: 16319201]

Zhang LI, Bao S, Merzenich MM. Persistent and specific influences of early acoustic environments on primary auditory cortex. Nat Neurosci 2001;4:1123–1130. [PubMed: 11687817]

Zhang LI, Tan AY, Schreiner CE, Merzenich MM. Topography and synaptic shaping of direction selectivity in primary auditory cortex. Nature 2003;424:201–205. [PubMed: 12853959]

Zhang ZW, Deschênes M. Intracortical axonal projections of lamina VI cells of the primary somatosensory cortex in the rat: a single-cell labelling study. J Neurosci 1997;17:6365–79. [PubMed: 9236245]

Zhang Y, Suga N. Corticofugal amplification of subcortical responses to single tone stimuli in the mustached bat. J Neurophysiol 1997;78:3489–3492. [PubMed: 9405567]

Zhang Y, Suga N. Modulation of responses and frequency tuning of thalamic and collicular neurons by cortical activation in mustached bats. J Neurophysiol 2000;84:325–333. [PubMed: 10899207]

Zhang Y, Yan J. Corticothalamic feedback for sound-specific plasticity of auditory thalamic neurons elicited by tones paired with basal forebrain stimulation. Cereb Cortex 2008;18:1521–1528. [PubMed: 18203697]

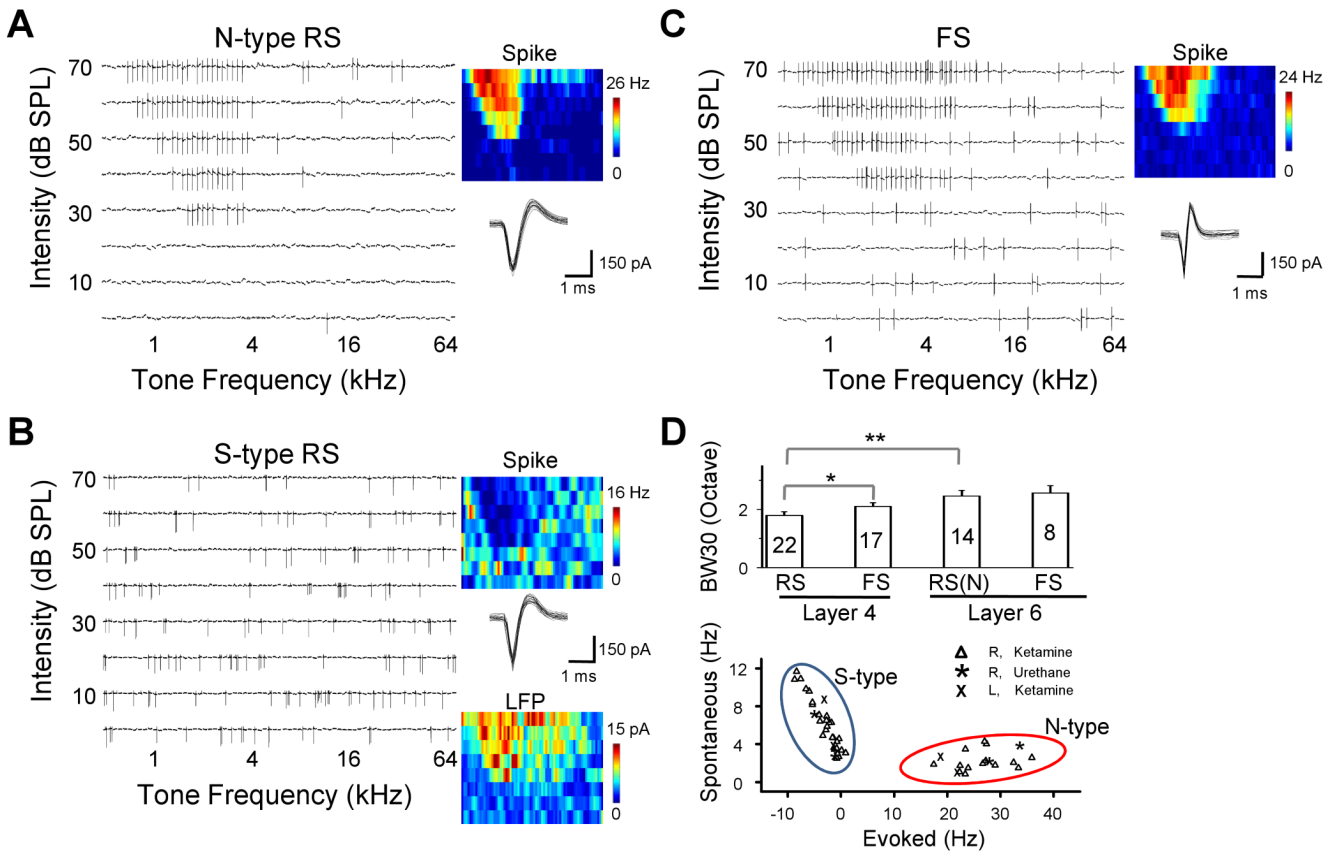

Figure 1.

Spike TRFs of individual neurons in layer 6 of the rat A1.

(**A**) An example normal-type (N-type) neuron as determined by cell-attached recording. Left, spike TRF mapped in one trial. Each small trace (100 ms) in the frequency-intensity space represents the response of the cell to a tone of a particular frequency and intensity. Right, the color map displays the cell's spike TRF with the color representing the average firing rate. Twenty randomly selected individual spikes are superimposed below the color map. The cell is a typical regular-spike (RS) neuron according to the spike shape.

(**B**) An example silent-type (S-type) neuron. Data are presented in the similar manner as in (**A**). TRF of local field potential (LFP) at recording site is displayed below the corresponding spike TRF. Note that both N- and S-type neurons are only defined for regular-spike pyramidal neurons.

(**C**) An example fast-spike (FS) interneuron. Note that the interval between the negative and positive peaks of the spike shape is shorter than that of regular-spike neurons.

(**D**) Upper panel, average bandwidth (responding frequency range) of spike TRFs for different types of neurons in layer 4 and 6. Bandwidth was measured at 30 dB above the threshold intensity of the TRF (BW30). The numbers of cells are indicated. RS(N): regular-spike normal-type neuron. Bar represents SEM. *, $p < 0.1$; **, $p<0.002$, ANOVA and post hoc Scheffe test. Lower panel, average rate of spontaneous and tone-evoked spikes (after subtraction of the basal level activity) of all the recorded RS neurons in layer 6. The evoked firing rate was averaged from responses at the characteristic frequency (CF) at from 20 dB above intensity threshold to 70 dB SPL. The CF was determined by the TRF of local field potentials in the case of silent-type neurons. Cells recorded under different anaesthesia are indicated. R and L indicate that

recordings were made in the right and left hemisphere, respectively. Tone stimuli were always applied to the contralateral ear. Clustering (N- and S- type) is based on K-means method.

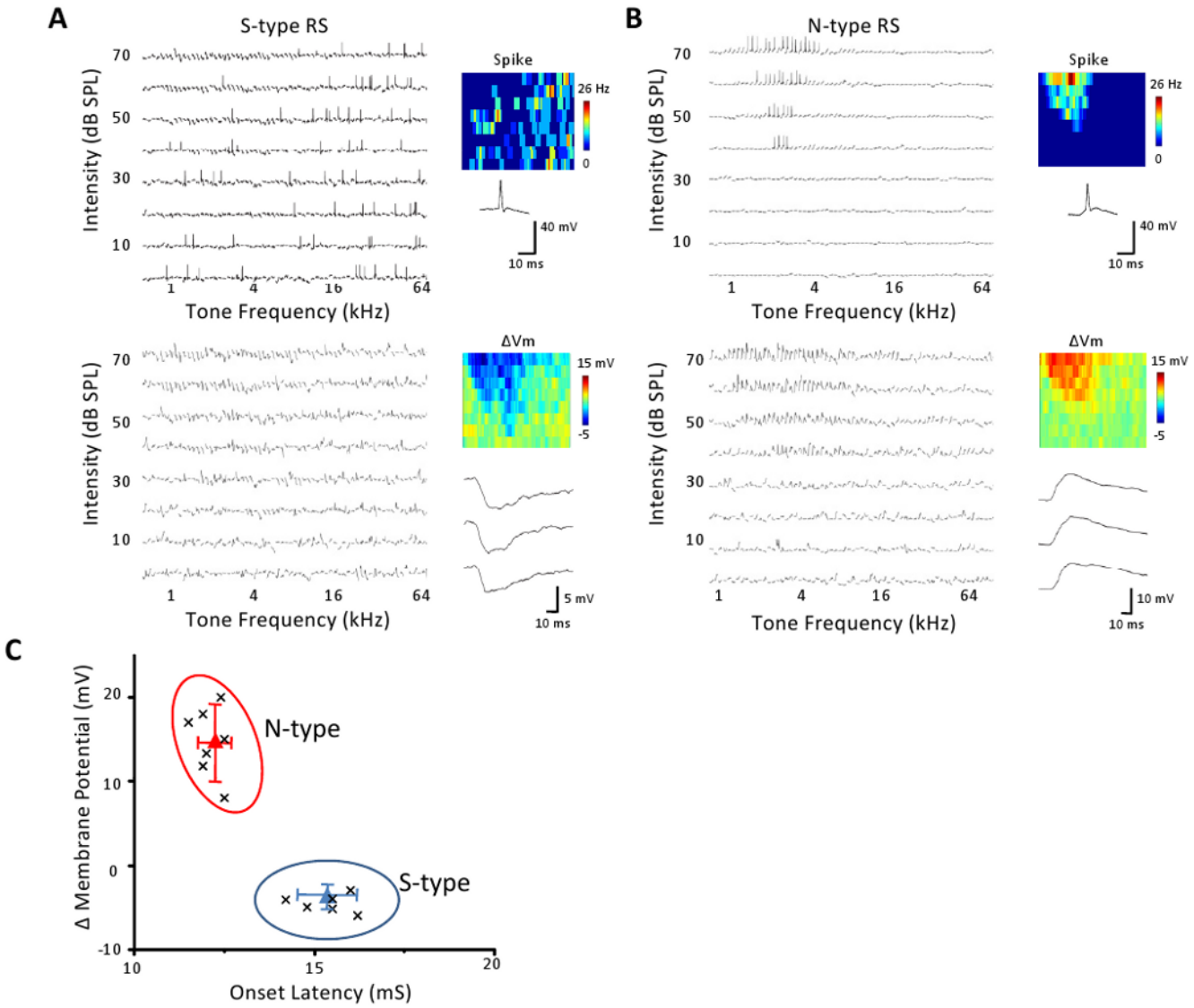

Figure 2.

Membrane potential TRFs of the two types of excitatory neurons in layer 6.

(**A**) An example silent-type neuron. Upper left, spike TRF mapped in one trial. Each small trace is a 100 ms response trace under current-clamp mode. Upper right, color map displays the spike TRF with the color representing the average firing rate. An example spike is shown below. Lower panel, membrane potential responses with the spikes removed (using a 10 ms median filter). Color represents the average peak amplitude of the evoked membrane potential change. Three enlarged response traces are shown.

(**B**) An example normal-type neuron. Data are presented in the same manner as in (**A**).

(**C**) The peak amplitude of evoked membrane potential change versus the response onset latency. Each data point represents one cell. Response to tone at the best frequency at 70 dB was measured. Clustering is based on K-means method. Triangle is the clustering center and whiskers are the corresponding standard deviation from the center.

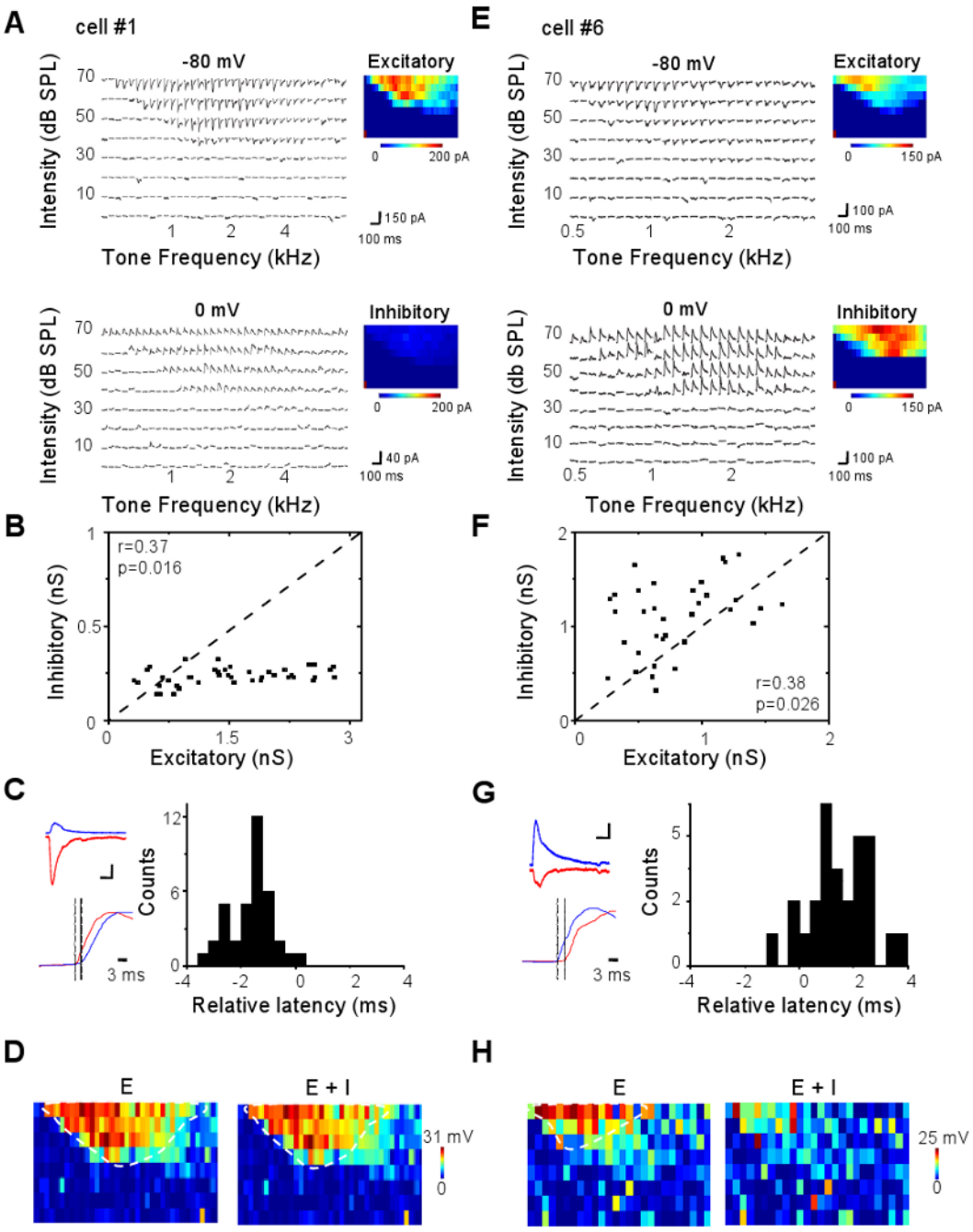

Figure 3.

Excitatory and inhibitory synaptic TRFs of example layer 6 neurons.

(**A**) A putative normal-type neuron (cell #1). Left, small traces are excitatory and inhibitory synaptic currents recorded under -80 mV (upper) and 0 mV (lower) respectively, in response to tones of various frequencies and intensities. Right, color represents the peak amplitude of the evoked synaptic current.

(**B**) The peak amplitude of inhibitory conductance versus that of the excitatory conductance activated by the same tone stimulus, plotted for cell #1. Data are from the responses to 70 dB tones at various effective frequencies. Dash line is the unity line. r, correlation coefficient; p, correlation significance.

(**C**) Left, top, average excitatory (red) and inhibitory (blue) currents of cell #1 in response to the tone at 70 dB and the best frequency. Scale: 50 pA and 50 ms. Bottom, comparison of the rising phases of the two synaptic responses (30ms trace). The excitatory response is reversed in polarity and normalized in amplitude. Two dotted lines indicate the onset timings. Right, distribution of relative latency (i.e. the difference between the onset latencies of excitatory and inhibitory responses, $\Delta t = T_E - T_I$) for cell #1's responses to 70 dB tones at various effective frequencies.

(**D**) TRF of membrane potential responses derived from excitatory input only (left) and by integrating excitatory and inhibitory inputs (right) for the cell #1. Color represents the peak amplitude of the membrane potential response. The resting membrane potential of the cell was -65 mV, and 20 mV above the resting potential was set as the spike threshold. The estimated spike response region is outlined by the dashed curve.

(**E-H**) A putative silent-type neuron (cell #6). Data are presented in the same manner as in (**A-D**). Scale: 50 pA and 50 ms in (**G**).

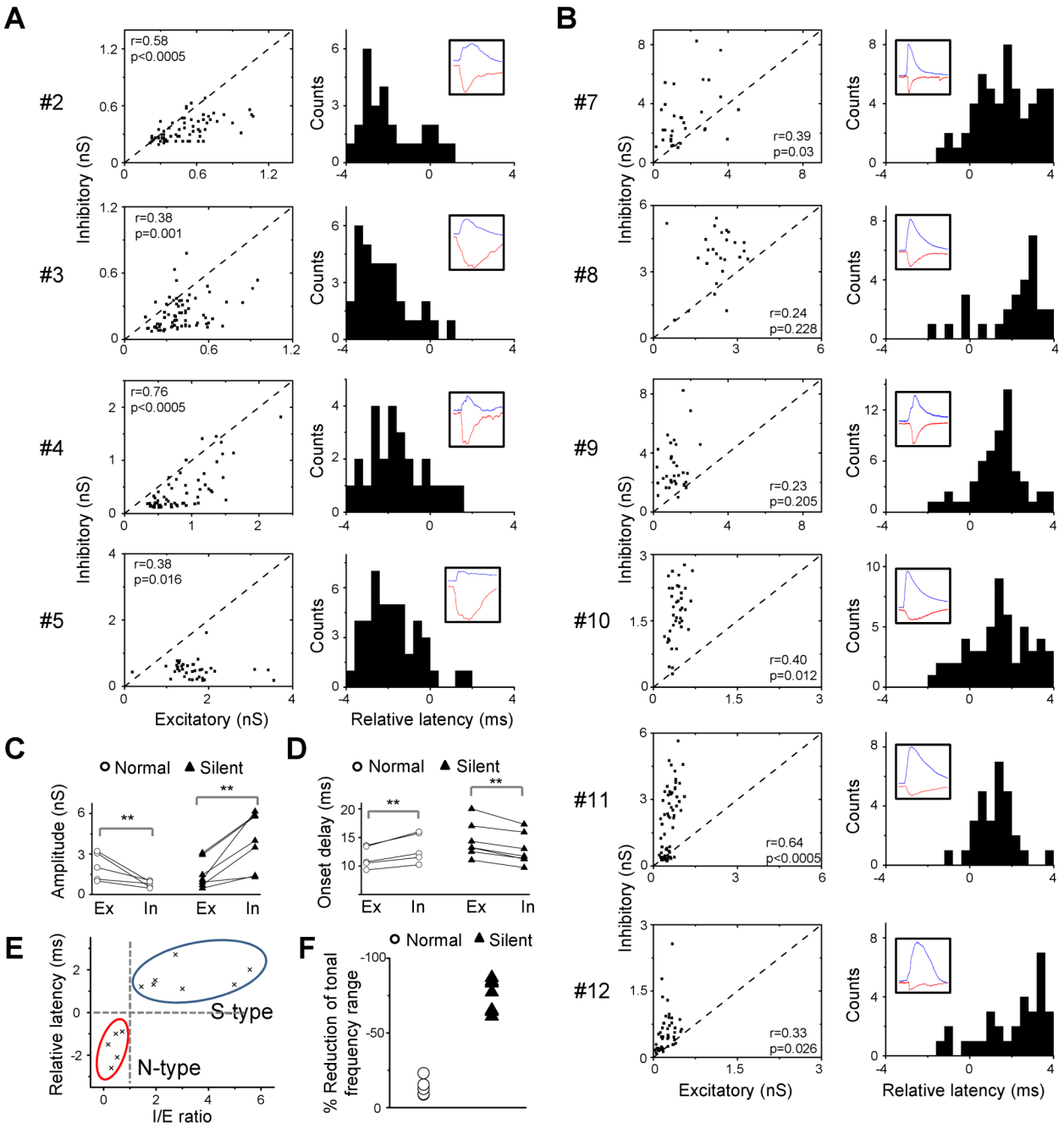

Figure 4.

Synaptic TRF properties of normal- and silent-type neurons in layer 6.

(**A**) Four other putative normal-type neurons (cell numbers are indicated on the left). Left, the peak amplitude of inhibitory conductance versus that of the excitatory conductance activated by the same stimulus for effective tones at 70 dB. Right, distribution of relative latency of for the same set of responses. Inset, example excitatory (red) and inhibitory (blue) responses. Each trace is an average of three responses to 70 dB tones at or near the best frequency.

(**B**) Six other putative silent-type neurons. Data are presented in the same manner as in (**A**).

(**C**) Average peak amplitudes of excitatory (Ex) and inhibitory (In) conductances evoked by three 70 dB tones at and near the best frequency. Data points for the same cell are connected by a line. **, $p < 0.01$, paired t-test.
(**D**) Average onset latencies of excitatory and inhibitory conductances as in (**C**). **, $p < 0.01$, paired t-test.
(**E**) The relative latency versus the ratio between the peak amplitudes of evoked inhibitory and excitatory conductances (I/E ratio), based on the data shown in (**C**) and (**D**). Clustering is based on K-means method.
(**F**) The percentage reduction of the total frequency responding range of spike responses after integration of inhibition. Comparison was made between spike responses to 70 dB tones derived from excitation alone and by integrating both excitation and inhibition.

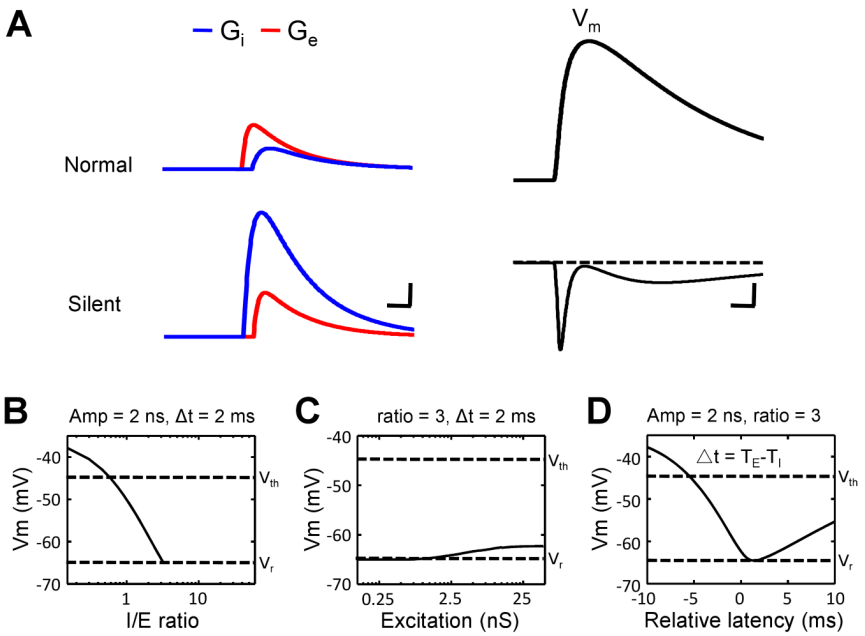

Figure 5.

Modeling the impacts of excitatory and inhibitory inputs on membrane potential responses. (**A**) Left, temporal profiles of the evoked excitatory (red) and inhibitory (blue) conductances used in the model (see Experimental Procedures). The peak conductances are 2 nS (red)/1 nS (blue) for an average normal-type neuron and 2 nS (red)/6 nS (blue) for a silent-type neuron. Scale: 1 nS and 5 ms. Right, temporal profiles of the membrane potential responses (V_m) derived by integrating the excitatory and inhibitory inputs. Scale: 3mV (upper)/1mV (bottom), 10 ms.

(**B**) The peak amplitude of the evoked membrane depolarizing response versus the relative level of inhibition. V_m represents the peak amplitude of the depolarization in the simulated membrane potential response. The peak excitatory conductance was set at 2 nS, and the relative latency was set at 2 ms. Two dashed lines mark the level of the resting membrane potential (V_r) and the spike threshold (V_{th}). Responses below the V_r are omitted.

(**C**) The level of membrane depolarizing response versus the strength of the excitatory input. The I/E ratio was set at 3, and the relative latency was set at 2 ms.

(**D**) The level of membrane depolarizing response versus the relative latency. The strengths of excitatory and inhibitory inputs were fixed at 2 and 6 nS respectively.

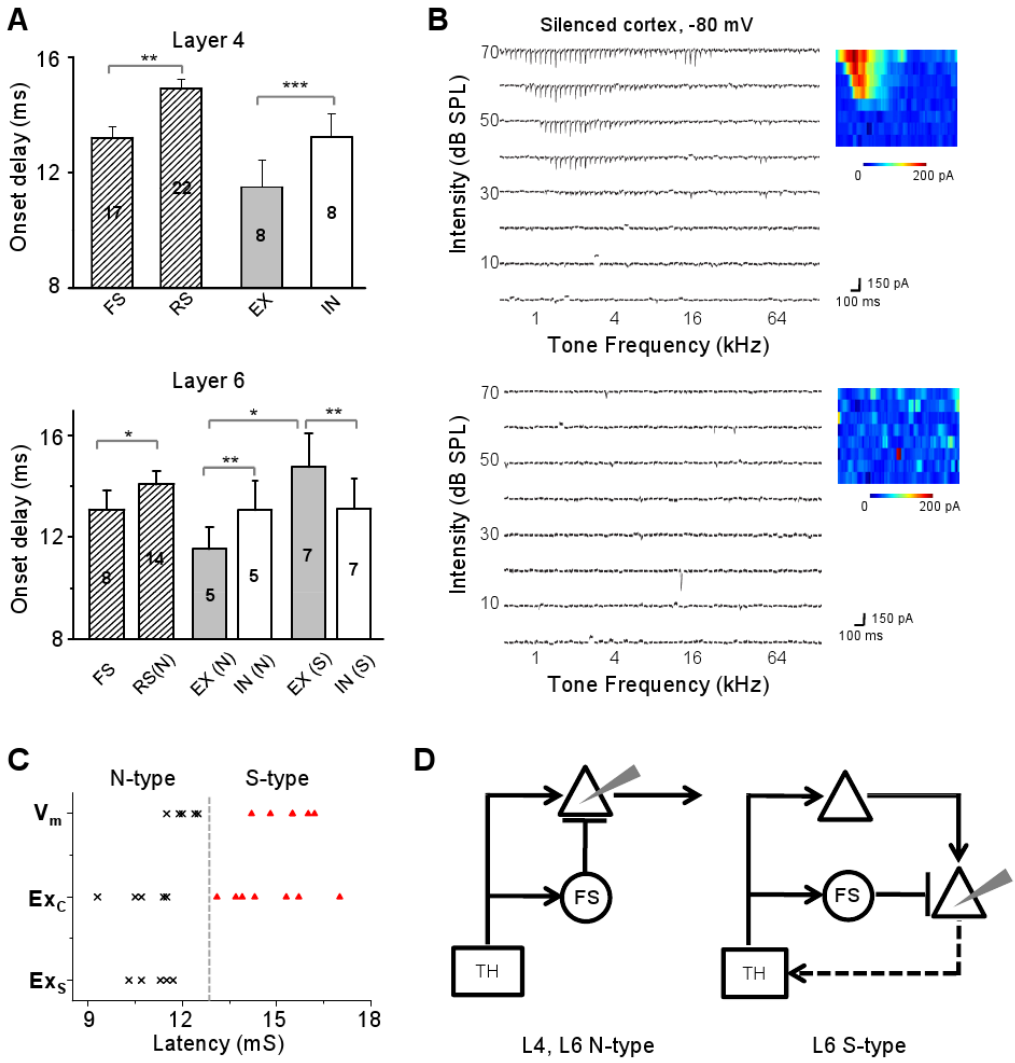

Figure 6.

Onset latencies of spike and synaptic responses of layer 4 and layer 6 neurons.

(**A**) Top, average onset latencies of spike responses (shaded bars) of layer 4 RS excitatory neurons and FS inhibitory neurons, as well as of the excitatory (grey bar) and inhibitory responses (white bar) of excitatory neurons. Bar = SEM. **, $p<0.01$, t-test. ***, $p<0.001$, paired t-test. Bottom, onset latencies for layer 6 neurons, presented in a similar manner as in (**A**). *, $p<0.05$, t-test. **, $p<0.01$, paired t-test. “N”, “S” and “FS” refer to the normal-type excitatory, silent-type excitatory and fast-spike inhibitory neurons respectively.

(**B**) Excitatory TRFs of two example layer 6 neurons recorded in the silenced cortex.

(**C**) Distribution of onset latencies of the membrane potential response (Vm) and excitatory response in the control cortex (Ex_C), as well as the excitatory response in the silenced cortex (Ex_S). Putative normal-type and silent-type neurons are represented by cross and triangle marks respectively.

(**D**) Left, schematic drawing of canonical feedforward circuit for recorded layer 4 neurons and layer 6 normal-type neurons (recording electrode is drawn in grey). TH, thalamus. Triangle, excitatory neurons. Circle, FS inhibitory neurons. Arrow head, excitatory connection. Bar, inhibitory connection. Right, proposed parallel feedforward circuit for recorded layer 6 silent-type neurons. At least some of these neurons project back to the thalamus.